Environ Earth Sci
DOI 10.1007/s12665-015-4054-y

ORIGINAL ARTICLE

Suitability of ANN applied as a hydrological model coupled with statistical downscaling model: a case study in the northern area of Peninsular Malaysia

Zulkarnain Hassan · Supiah Shamsudin · Sobri Harun · Marlinda Abdul Malek · Nuramidah Hamidon

Received: 31 December 2013 / Accepted: 10 January 2015

Abstract The increase in global surface temperature in response to the changing composition of the atmosphere will significantly impact upon local hydrological regimes and water resources. This situation will then lead to the need for an assessment of regional climate change impacts. The objectives of this study are to determine current and future climate change scenarios using statistical downscaling model (SDSM) and to assess climate change impact on river runoff using artificial neural network (ANN) and identification of unit hydrographs and component flows from rainfall, evaporation and streamflow data (IHACRES) models, respectively. This study investigates the potential of ANN to project future runoff influenced by large-scale atmospheric variables for selected watershed in Peninsular Malaysia. In this study, simulations of general circulation models from Hadley Centre 3rd generation with A2 and B2 scenarios have been used. According to the SDSM projection, daily rainfall and temperature during the 2080s will increase by up to 2.23 mm and 2.02 °C, respectively. Moreover, river runoff corresponding to downscaled future projections presented a maximum increase in daily river runoff of 52 m^3/s. The result revealed that the ANN was able to capture the observed runoff, as well as the IHACRES. However, compared to the IHACRES model, the ANN model was unable to provide an identical trend for daily and annual runoff series.

Keywords Statistical downscaling · IHACRES · Artificial neural network · River runoff · Malaysia

Z. Hassan (✉) · S. Harun · N. Hamidon
Faculty of Civil Engineering (FKA), Universiti Teknologi Malaysia (UTM), 81310 Skudai, Johor, Malaysia
e-mail: zulkarnain.hassan87@gmail.com; zulkarnain23@live.utm.my

Z. Hassan
School of Environmental Engineering, Universiti Malaysia Perlis, Kompleks Pusat Pengajian Jejawi 3, 02600 Arau, Perlis, Malaysia

S. Shamsudin
Razak School of Engineering and Advanced Technology, Universiti Teknologi Malaysia-Kuala Lumpur, 54100 Kuala Lumpur, Malaysia

M. A. Malek
Department of Civil Engineering, College of Engineering, Universiti Tenaga Nasional, 43000 Kajang, Selangor, Malaysia

Introduction

The effects of climate change upon the areas of hydrology and water resources have become an important topic for research and discussion over the past few decades. It is believed that the subject of climate change has significant implications for the environment, ecosystems, water resources and all aspects of human life, respectively (Jiang et al. 2007). In hydrology, possible effects of global warming include: (1) changes in magnitude and timing of rainfall and runoff; (2) changes in the frequency and intensity of droughts and floods, and; (3) changes relating to the quality and quantity of water (Nakićenović et al. 2000). In order to determine the impact of climate change, especially regarding changes in runoff, the relationships between them are analysed using the general circulation models (GCMs) output as proposed by Xu (1999). GCMs are considered as comprehensive models for investigating the physical and dynamic processes of the earth–atmosphere system, as well as providing plausible patterns of global climate change (Jiang et al. 2007).

The output of the GCMs has a coarse spatial resolution data and is therefore not suitable to be used directly for

Published online: 23 January 2015

hydrological assessment (Combalicer et al. 2010; Khan et al. 2006; Wilby and Wigley 1997). Xu (1999) and Dibike and Coulibaly (2005) recommended that the projection of runoff changes corresponding to the climate scenarios be used by applying the hydrological models along with the downscale rainfall and temperature from the coarse spatial resolution of GCMs. Although it is possible to directly downscale the GCMs model to runoff, any possible changes in the frequency and duration of climate series are not likely to be provided by a linear scaling (Xu 1999).

The downscale rainfall and temperature from GCMs are conducted by applying downscaling approaches. Two major approaches can be applied, namely statistical and dynamical downscaling approaches (Wilby et al. 2002). In this study, statistical downscaling approaches are utilized. These approaches use a method which derives local-scale information from GCMs through inference from the cross-scale relationship by using some random and/or deterministic functions (Coulibaly and Dibike, 2005). The main advantages of statistical downscaling approaches are that they are: (1) inexpensive; (2) computationally undemanding; and (3) readily transferable. This means that it is able to provide the local information that is most needed in many climate change impact applications. Further, ensembles of climate scenarios permit the use of risk or uncertainty analyses. The approaches are categorized into three types, specifically: (1) regression methods; (2) weather pattern-based approaches; and (3) stochastic weather generators.

The hybrid model named statistical downscaling model (SDSM) (Wilby et al. 2002), which utilizes regression and stochastic weather generators, has been used. As reviewed by Wilby and Dawson (2013), application of the SDSM model is becoming a model of interest to be used in downscaled meteorological variables. In addition, it is being intensively studied throughout the world. However, only a few explorations into the SDSM model have been studied in Malaysia. Tukimat et al. (2012) explored the potential of the SDSM model when estimating potential evapotranspiration at an irrigation scheme in the northern area of Peninsular Malaysia. Meanwhile, Hassan et al. (2014a) compared the application of the SDSM model with the Long Ashton Research Station Weather Generator (LARS-WG) which utilized stochastic weather generators over the entire area of Peninsular Malaysia. Their studies found that the SDSM and LARS-WG models are able to capture the present climate series, although they have not given an indication of an identical trend of the future climate series. Kabiri et al. (2014) also applied the SDSM model with the HEC-HMS hydrological model in order to project the future discharge of the Klang River catchment located at the centre of Peninsular Malaysia. Their assessment found an increase in river discharge rate recorded in the studied catchment area by using rainfall and temperature turbulent together with the climate scenarios.

In terms of simulating runoff or discharge corresponding to the climate scenarios, the following conclusion was reached. Despite the artificial neural networks (ANNs) being successfully applied as the hydrological model (e.g. Zadeh et al. 2010; Nor et al. 2007; and Dibike and Solomatine 2001), these models were not widely applied in the climate change assessment. A few explorations on the subject of integration between the downscaled GCMs and ANNs as the hydrological model (e.g. Zarghami et al. 2011) have been recorded. However, comparison and evaluation between the ANN model and the hydrological models which utilized conceptual and physical models have not been well discussed. Therefore, this evaluation can be regarded as a research interest into this study in relation to the studied region.

In this study, it is proposed to apply identification of unit hydrographs and component flows from rainfall, evaporation and streamflow data (IHACRES), with the result becoming a benchmark for the result of the ANN model. IHACRES is a hybrid rainfall-runoff model in which metric and conceptual models are utilized (Croke and Jakeman 2004). It has been reported that it can be applied to a catchment with a wide range of sizes and climatologies (Croke and Jakeman 2004). IHACRES has been used to predict runoff in the un-gauged catchment, as well as to investigate dynamic response characteristics and the physical catchment (Kokkonen et al. 2003). Due to the minimal data requirement, IHACRES has been successfully used in many catchments and responses (Bernard et al. 2013) as well as in the climate change assessment such as Karamouz et al. (2012), Samadi et al. (2012, 2013) and Zareian et al. (2014).

This paper aims to identify the potential of the ANN model as the hydrological model by which to project the river runoff corresponding to climate change. The anticipated future rainfall and temperature data were generated by using the SDSM model. The IHACRES method was applied to simulate the river runoff from rainfall and temperature data, and it was subsequently compared with the ANN projection. In the following sections, the case study is introduced and followed by the methodology of the study. The results and discussions are then imparted, and finally, the conclusions are presented.

Study watershed and input data

Study watershed

The sub-catchment area of the Kurau River was chosen as the study watershed. It is located in the northern area of

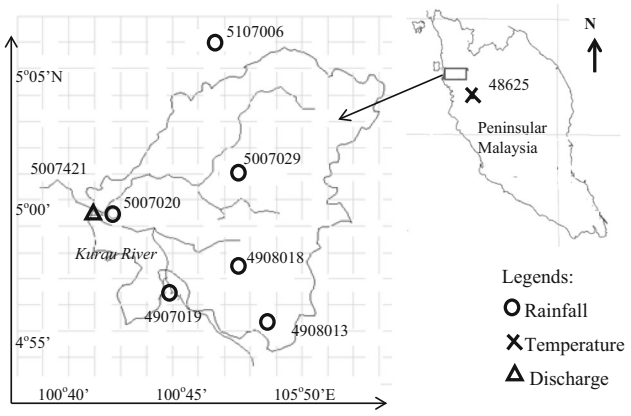

Fig. 1 Location of study area

Peninsular Malaysia in the state of Perak. The delineated study watershed is shown in Fig. 1. The watershed was selected since a dam (Bukit Merah reservoir) is located at the downstream of the basin. This dam acts as the main water resource for the Kerian irrigation scheme, as well as being the main source of domestic water supply for the Kerian and Larut Matang districts in Perak. Assessing the impact of climate change may provide an insight into appropriate decisions in the future concerning the location of water resources development at the study watershed.

The sub-basin has an area of approximately 337 km^2 and is covered with palm oil estates, rubber farms, forests and a small residential area. The river originates partly from the Bintang Range, where the upper terrain reaches are steep and mountainous. The ground elevation at the river headwaters is moderately high, with 1,200 and 900 m heights in Batu Besar and Batu Ulu Trap, respectively.

Input data

The daily time series data for rainfall and runoff, which are used in this study, were obtained from the Department of Irrigation and Drainage Malaysia, while the temperature data were obtained from the Malaysian Meteorological Department. The location and details of rainfall and river runoff are shown in Fig. 1 and Table 1, respectively. Since there is no temperature station in the study watershed, a nearby temperature station (details as in Table 1) in Ipoh, Perak was chosen. The study assumes that the temperature in Ipoh is the same as in the area of study catchment. Although the Ipoh temperature station is measured with a difference of about half a degree, it is still tolerable since the temperature difference between stations in the Peninsular Malaysia area is small. It has a uniform warming, and there is an insignificant difference between each location (Hassaballa and Matori 2011). All data contain a smaller missing value (<5 %). The missing value of rainfall and temperature was filled using PASW Statistics version 18 (SPSS Inc., Chicago, IL, USA) by the expectation–maximization algorithm and the correlation of nearby observed stations.

In relation to a future climate change impact study, the large-scale predictors of Hadley Center's GCM (HadCM3) with A2 and B2 scenarios run for 1961–2099 and reanalysis data predictors of the National Center of Environmental Prediction (NCEP) on HadCM3 computational grid for 1961–2000 at daily time step have been used in the study (as shown in Table 2). HadCM3 is a coupled atmosphere–ocean GCM developed at Hadley Centre United Kingdom National Meteorological Service. This GCM contains a complex model of land surface processes, including: (1) 23 land cover classifications; (2) four layers of soil where temperature, freezing and melting points are tracked; and (3) a detailed evapotranspiration function that depends on temperature, vapour pressure, vegetation type and ambient carbon dioxide concentrations (Hassan and Harun 2012). HadCM3 was chosen since the model is widely used in many climate change impact studies (such as Wilby 2005; Wilby and Harris 2006; Chu et al. 2010; Mollema et al. 2012). Furthermore, HadCM3 provides daily predictor variables, which can be used for the SDSM model. It was run for over 1,000 years, showing a little drift in its surface climate (Gordon et al. 2000). In this

Table 1 Details of runoff and meteorology stations

Number of station	Name of station	Type of station	Location	
			Lat. (° ′ ″)	*Long.* (° ′ ″)
5007421	Sg. Kurau, Pondok Tanjung	Runoff	5 00 46	100 43 55
5007020	Sg. Kurau, Pondok Tanjung	Rainfall	5 00 42	100 34 52
5007029	Ibu Bekalan Jelai	Rainfall	5 01 20	100 48 00
5107006	Ldg. Stoughton, Batu Kurau	Rainfall	5 06 25	100 46 20
4907019	Ldg. Norseman	Rainfall	4 57 55	100 45 50
4908013	Ibu Bekalan Sempeneh	Rainfall	4 56 05	100 49 40
4908018	Pusat Kesihatan Kecil	Rainfall	4 58 45	100 48 15
48625	Ipoh, Perak	Temperature	4 34 01	101 06 00

Table 2 List of predictors from NCEP variables with high monthly correlation corresponding to each of the predictand

Variables	Description of variables	Rainfall			T_{max}			T_{min}		
		r	*Partial r*	*p* value	*r*	*Partial r*	*p* value	*r*	*Partial r*	*p* value
mslp	Mean sea level pressure	−0.026	−0.114	0.000						
p_f	Surface airflow strength				0.049	0.009	0.452	0.004	0.034	0.023
p_thas	Surface wind direction				−0.025	−0.076	0.000	−0.255	−0.135	0.000
p_z	Surface vorticity							0.057	0.022	0.156
p500	500 hPa geopotential height				0.111	0.134	0.000	0.150	0.114	0.000
p5thas	500 hPa wind direction	0.079	0.036	0.074						
p8_f	850 hPa geostrophic air flow velocity	−0.062	−0.034	0.096						
p8_z	850 hPa vorticity	0.088	0.054	0.006	0.191	0.119	0.000			
p850	850 hPa geopotential height	−0.014	0.098	0.000						
p8thas	850 hPa wind direction	0.074	0.100	0.000						
p8z	850 hPa divergence	0.036	0.041	0.039						
rhum	Near surface relative humidity	0.197	0.198	0.000						
shum	Surface specific humidity				−0.123	−0.141	0.000	0.246	0.102	0.000
tempas	Mean temperature at 2 m				0.382	0.342	0.000	0.302	0.177	0.000

study, two climate scenarios based on the HadCM3 were applied, named as A2 and B2. The A2 is considered among the "worst" case scenarios, projecting high emissions for the future. Conversely, it was found that B2 would project lower emissions in the future and, accordingly, is considered as an "environmental" case scenario.

The reanalysis data predictor of the National Center of Environmental Prediction (NCEP reanalysis) has been developed by the National Center for Environmental Prediction (US). The data are used for examining observed relationships between atmospheric and surface variables at regional to continental scale within the historical meteorological data (Poccard et al. 2000; Kalnay et al. 1996). These relationships are important by which to produce climate scenarios downscaled from other climate model outputs (Kaas and Frich 1995). Reanalysis data contribute to the following, namely climate predictability, system performance observation, general circulation diagnostics, atmospheric low-frequency variability, the global hydrological and energy cycle and coupled ocean–atmosphere modelling (Gibson et al. 1999). Since HadCM3 A2 and NCEP reanalyses exhibit differences in grid and coarseness, the NCEP data were normalized and interpolated to the same grid as HadCM3 A2 (2.5° latitude × 3.75° longitude). The equation of normalization of NCEP data is written as;

$$\hat{u}_t = \frac{u_t - \bar{u}}{\sigma_u}$$

in which $\hat{u}_t$ is the normalized atmospheric variable at time t, u_t is the original data at time t, $\bar{u}$ is the multiyear average during the period, and σ_u is the standard deviation (Chu et al. 2010). The full data of HadCM3 with A2 and B2 scenarios and NCEP can be downloaded at http://www.cccsn.ec.gc.ca/index.php?page=dst-sdi.

Methodology

The methodology of this study consists of two important steps, which are to, namely (1) downscale the GCM data for the province under different emission scenarios by using the SDSM; and (2) assess the impacts of climate change on the streamflow by using the ANN and IHACRES models. In the following sections, the methods and models used in this study are described.

SDSM model

The SDSM model is introduced by Wilby et al. (2002). It builds up the relationship between the GCMs' variables (known as predictors) and the local-scale variables (known as predictands) (Chu et al. 2010), as:

$$Y = F(X) \tag{2}$$

in which Y means the local predictand and, $X(x_1, x_2, \ldots, x_n)$ represents n large-scale atmospheric predictors, and F is the built quantitative statistical relationship.

The SDSM method consists of two steps. The first step determines whether rainfall occurs on each day or not. The equation for the first step is written as,

$$w_t = \propto_0 + \sum_{j=1}^{n} \propto_j \hat{u}_t^{(j)} + \propto_{t-1} w_{t-1} \tag{3}$$

in which t is time (days), w_t is the conditional possibility of rain occurrence on day t, $\hat{u}_t^{(j)}$ is the normalized predictor, α_j is the regression parameter deduced by an ordinary least square method, and w_{t-1} and α_{t-1} are the conditional probabilities of rain occurrence on day $t-1$ and lag-1 day regression parameter, respectively. These two parameters are optional, depending on the studied region and predictand. Uniformly, distributed random number r_t $(0 \le r_t \le 1)$ is used to determine the rain occurrence and the possibility that the rain would happen if $w_t \le r_t$.

The second step determines the estimated value of rainfall on each rainy day. This can be represented with a z-score;

$$Z_t = \beta_0 + \sum_{j=1}^{n} \beta_j \hat{u}_t^{(j)} + \beta_{t-1} + \varepsilon \tag{4}$$

in which, Z_t is the z-score on day t, β_j is the calculated regression parameter, and β_{t-1} and Z_{t-1} are the regression parameters and the z-score on day $t-1$, respectively. Basically, rainfall y_t on day t can be written as;

$$y_t = F^{-1}[\emptyset(Z_t)] \tag{5}$$

in which, $\emptyset$ is the normal cumulative distribution function, and F is the empirical function of y_t. For the daily temperature analysis, Eq. 3 is not applied since the stochastic amount is not considered.

The large-scale predictors (among those presented in Table 2) for the meteorological prediction employing the SDSM model used in this study were based on the output from the NCEP reanalysis for calibration, as well as HadCM3 A2 and B2 for future generation.

IHACRES model

The IHACRES Classic Plus (Croke et al. 2006) model utilized in this study can be downloaded for free at (http://www.toolkit.net.au/Tools/IHACRES) to provide an enhancement of the IHACRES_PC software (Littlewood et al. 1997). This model is based on the concept of modelling identifiable catchment-scale rainfall-runoff behaviour that causes runoff. It includes a series of two modules, which are the nonlinear loss module and linear unit hydrograph modules, respectively (Croke and Jakeman 2004). With regard to rainfall, r_k, due to time step, k, will be transformed into an effective rainfall, u_k thereby leaving a catchment as runoff, x_k. This transformation is similar to the concept of unit hydrograph theory, which is a configuration of linear storage acting in series and/or parallel in the catchment.

The nonlinear module of Ye et al. (1997) is used to calculate the effect of antecedent weather conditions on both, the current status ($\emptyset_k$) of soil moisture and vegetation conditions, and for evapotranspiration effects. The u_k is calculated using the formula:

$$u_k = [c(\emptyset_k - 1)]^p r_k \tag{6}$$

$$\emptyset_k = r_k + \left(1 - \frac{1}{\tau_w(t_k)}\right) s_{k-1} \tag{7}$$

$$\tau_w(t_k) = \tau_w \exp[0.062 f(T_r - T_k)] \tag{8}$$

in which, $\emptyset_k$ is the soil moisture index. A function of t_k, the evaporation at time k, and the dynamic response characteristics (τ_w, f, c, T_r) are used to calculate the excess rainfall for each time step. It represents the extent to which the catchment is saturated. The τ_w is a time constant for the decline in the catchment wetness index. The f is the parameter that regulates the degree of evaporation dependence of the lost time constant, while c is used to conserve the mass balance of the catchment and T_r indicates a reference temperature. The parameter τ_w reflects the rate of drying of the catchment at 20 °C.

The linear module uses a transfer function to allow effective rainfall to pass through any combination of stores, in parallel and series, in order to become runoff. Commonly, it uses a configuration of two stores in parallel except in semi-arid regions, or for ephemeral streams, where often one store is sufficient. In the module, the function x_k^q indicates the quickflow (surface runoff), and the x_k^s function refers to the slow flow (base flow). These functions are combined to yield the runoff, x_k expressed as follows:

$$x_k = x_k^q + x_k^s \tag{9}$$

where

$$x_k^q = -\alpha_q x_{k-1}^q + \beta_q u_k \tag{10}$$

$$x_k^s = -\alpha_s x_{k-1}^s + \beta_s u_k \tag{11}$$

The parameters α_q and α_s are time constants for the quick and slow flow stores. The optimum configuration for each parameter is summarized in Table 3.

Artificial neural network

The ANN architecture of the multilayer perceptron (MLP) neural network model was also used in this study. This ANN model architecture has been widely used in the field of hydrology (Hsu et al. 1995; Tokar and Johnson 1999; Dawson and Wilby 2001; Zhang and Savenije 2005), particularly for runoff analysis (Minns and Hall 1996). The MLP network utilizes the two-layer feed forward network trained with back-propagation learning algorithm. The transfer function used in the hidden layer is tan-sigmoid (*tansig*) and linear transfer function (*purelin*) at the output layer. The neurons in each layer are connected to the

Table 3 Optimum configuration of the IHACRES model

List of IHACRES parameter	Value
Nonlinear model module	
Mass balance term (c)	0.000035
Drying rate at reference temperature (t_w)	27
Temperature dependence of drying rate (f)	1
Reference temperature (t_{ref})	20
Moisture threshold for producing flow (l)	0
Power on soil moisture (p)	1
Linear model module	
Recession rate 1 ($\alpha^{(s)}$)	−0.998
Recession rate 2 ($\alpha^{(q)}$)	−0.623
Peak response 1 ($\beta^{(s)}$)	0.001
Peak response 2 ($\beta^{(q)}$)	0.217
Time constant 1 ($\tau^{(s)}$)	537.893
Time constant 2 ($\tau^{(q)}$)	2.115
Volume proportion 1 ($v^{(s)}$)	0.423
Volume proportion 2 ($v^{(q)}$)	0.577

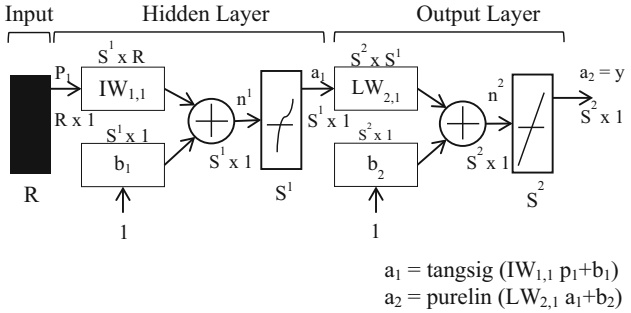

Fig. 2 MLP network architecture

neurons in the subsequent layer by a weight which is adjusted during training. Figure 2 exhibits the MLP network architecture.

As shown in Fig. 3, the input vector, $p1$, is propagated towards the hidden layer by the multiplication of input weight matrices, $IW_{1,1}$ to form $IW_{1,1}p1$. Then, the sum of bias, b_1 and the product of $IW_{1,1}p1$ are propagated forward to *tansig* transfer function. This sum is passed through *tansig* transfer function so as to obtain the hidden neurons' output a_1, where $a_1 = tansig(IW_{1,1}p1+b1)$. Similarly, the output a_1 from the hidden layer is propagated forward through the network towards the output layer. At the output layer, a_1 is multiplied with the weight matrices in layer outputs, which are called layer weights, $LW_{2,1}$ to form $LW_{2,1}a_1$. Following this, the sum of bias b_2 and product $LW_{2,1}a_1$ will then be transformed through the *purelin* transfer function and neurons' output, a_2 where $a_2 = purelin(IW_{2,1}a1+b2)$. Subsequently, error signals that have been calculated by the feedback iteration will be propagated backwards through the network in order to adjust the weights of the output layer. Adjustments are made for interconnection weights between each layer based on the computer error and learning rate parameter. The summary of configuration of the MLP model is shown in Table 4.

The input data used for the MLP model consist of the following: the antecedent total daily rainfall $\{P(t-1), P(t-2),\ldots, P(t-n)\}$,the total rainfall $\{P(t)\}$, the antecedent mean daily temperature $\{T(t-1), T(t-2),\ldots, T(t-n)\}$ and the mean temperature of the current day $\{T(t)\}$. The output data refer to the simulated mean current daily runoff $\{Q(t)\}$. Through the preliminary study (Hassan et al. 2014b), only nine of the antecedent rainfall and temperature data (20 of daily series) were used due to quality and availability of input data, and were defined as:

$$Q(t) = f\{I\} \tag{12}$$

where

$$\begin{aligned} I = \{&P(t), P(t-1), P(t-2), P(t-3), P(t-4), P(t-5),\\ &P(t-6), P(t-7), P(t-8), P(t-9), T(t), T(t-1),\\ &T(t-2), T(t-3), T(t-4), T(t-5), T(t-6),\\ &T(t-7), T(t-8), T(t-9)\} \end{aligned} \tag{13}$$

Evaluation and statistical analysis

The performance during the calibration and validation of the SDSM was checked by using the statistical parameters, namely mean daily rainfall, maximum (T_{max}) and minimum (T_{min}) daily temperature for the whole month. Meanwhile, the performance of the ANN and IHACRES models was measured by using the coefficient of correlation (R), Nash–Sutcliffe efficiency (NSE) and root mean square error (RMSE) which can be defined as,

$$R = \frac{\sum(\text{obs} - \overline{\text{obs}})(\text{pred} - \overline{\text{pred}})}{\sqrt{\sum(\text{obs} - \overline{\text{obs}})^2 \sum(\text{pred} - \overline{\text{pred}})^2}} \tag{14}$$

$$\text{NSE} = 1 - \frac{\sum(\text{obs} - \text{pred})^2}{\sum(\text{obs} - \overline{\text{obs}})^2} \tag{15}$$

$$\text{RMSE} = \sqrt{\frac{(\text{obs} - \text{pred})^2}{n}} \tag{16}$$

inn which, obs = observed streamflow value; pred = predicted streamflow value; $\overline{\text{obs}}$ = mean streamflow observed value; and $\overline{\text{pred}}$ = predicted mean streamflow. The closer R and NSE values are to 1 and RMSE value is to 0, the better the prediction.

In relation to the trend analysis of the studied variables, there are two nonparametric methods which are used,

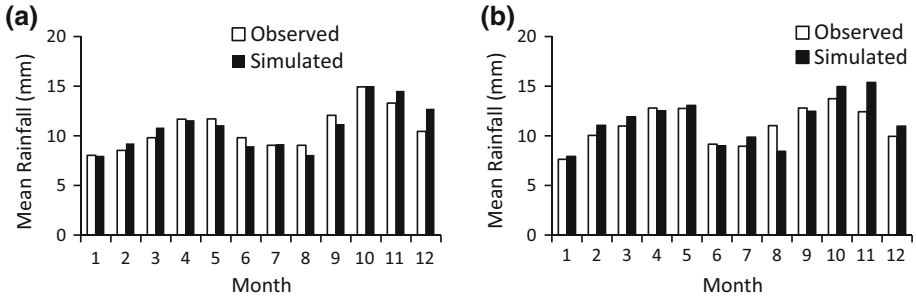

Fig. 3 Performance of the SDSM model on mean daily rainfall during **a** calibration (1966–1980) and **b** validation (1981–1995) periods

Table 4 Optimum configuration of the ANN model

ANN parameter	Value
Training algorithm	*TRAINSCG*
No. of neurons	125
Different learning training	0.8

specifically: Kendall's Tau-b (τ_b) (Kendall, 1938) and Sen's slope (Q_{med}) (Sen, 1968) estimator. At any sample of n pair of a bivariate variable (X, Y), there are $n(n-1)/2$ possible comparisons of (Xi, Yi) and (Xj, Yj). If C indicates the number of pairs that are concordant and D refers to the number of pairs that are discordant, then the τ_b can be defined as follow:

$$\tau_b = \frac{C - D}{\sqrt{(C + D + X_0)(C + D + Y_0)}} \tag{17}$$

where X_0 is the number of pairs tied only on the X variable and vice versa for Y_0. The full method of Kendall's Tau including Tau-b is well described by Kendall (1938) and Puka (2011).

The Q_{med} can be defined as follows:

$$Q_{\text{med}} = \begin{cases} Q_{[(N+1)/2]}, & \text{if} \quad N\text{isodd} \\ \dfrac{Q_{[(N+1)]} + Q_{[(N+1)/2]}}{2}, & \text{if} \quad N\text{iseven} \end{cases} \tag{18}$$

Where

$$Q_i = \frac{x_j - x_k}{j - k}, \quad \text{for} \quad i = 1, 2, \ldots N \quad \text{and} \quad j > k \tag{19}$$

The x_j and x_k are the data values at times j and k, respectively. The N values of Q_i are ranked from smallest to largest, and the median of slope or Q_{med} is computed as above. The Q_{med} sign reflects the data trend reflection, while its value indicates the steepness of the trend.

Results

Selection of predictand of the SDSM model

Table 2 presents the NCEP variables identified with monthly correlation between NCEP (named as predictor) and predictand variables (rainfall: 1966–1975 and temperature: 1968–1982). The selection of predictor is based on the higher correlation (r) and partial correlation (*partial r*) between each predictor and predictand variables. The significance value (*p value*) less than 0.05 becomes another criterion by which to select the predictor variable. There are several predictors for rainfall (such as mslp, p8_f, p850) that are not correlated with rainfall for reasons of either giving negative value of r and *partial r*, and not significant (*p value* >0.05). However, those predictors have been selected as the combination of predictors in the calibration of the SDSM model to describe intermediate process in the conditional process of rainfall. In relation to temperature, particularly maximum (T_{max}) and minimum (T_{min}) temperature, *tempas* has become the main predictor of the SDSM model to have been suggested in the previous study by the first author (Hassan et al. 2014a) in Peninsular Malaysia. Other predictors were selected along with *tempas* so as to enhance the quality of downscaling T_{max} and T_{min}, although *p_f* and *p_z* do not have a significant impact upon temperature.

Performance of the SDSM model

Figures 3, 4 and 5 show the SDSM performances for downscaling mean rainfall, T_{max} and T_{min}, respectively during the calibration and validation periods. The daily series of rainfall and temperature (T_{max} and T_{min}) from 1966–1975 to 1968–1982, respectively are utilized for the calibration period. For the validation period, rainfall and temperature data from 1976–1990 to 1983–1998 are set as the validation period, respectively. The figures indicate an acceptable performance between the observed and simulated predictands such as mean rainfall, T_{max} and T_{min} corresponding to NCEP-reanalysis predictors in the calibration and validation periods. The absolute differences between the observed and simulated mean daily rainfall in each month during the calibration period (Fig. 3a) are smaller, with the range of 0.04 (January) to 2.28 mm (December). A slight increase of differences was recorded during the validation periods (Fig. 3b), in which the range extended from 0.16 (June) to 2.95 mm (November). In the

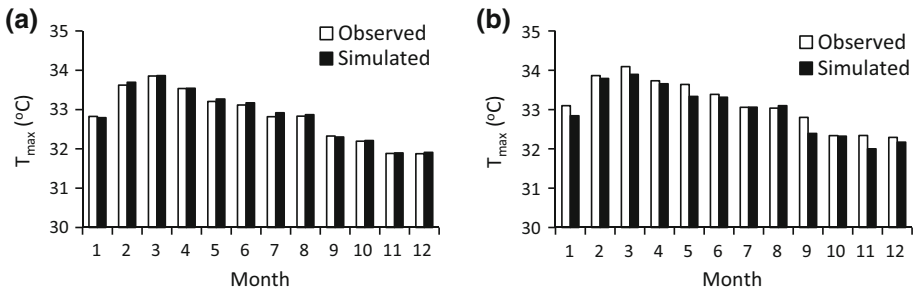

Fig. 4 Performance of the SDSM model on maximum daily temperature (T_{max}) during **a** calibration (1968–1989) and **b** validation (1989–2001) periods

case of downscaling daily T_{max} (Fig. 4), the differences are smaller with the ranges extending from 0.01 (March) to 0.10 °C (July) during the calibration period (Fig. 4a). During the validation period (Fig. 4b), the estimated T_{max} values are acceptable with the differences ranging from 0.00 (July) to 0.41 °C (September). This performance trend was not followed by the downscaling of T_{min} (Fig. 5), in which the validation result is slightly higher than the calibration result. The validation result of minimum temperature (wherein the difference between observed and simulated value is smaller, with the range of 0.8–1.0 °C) is still acceptable.

Performance of the ANN and IHACRES models

Table 5 demonstrates the performance of the ANN and IHACRES models during the model development when simulating runoff. The performance is checked using the comparative of the statistical characteristic [mean, standard deviation (SD), skewness and maximum] of observed and simulated data. Three performance indicators named as the *R* (Eq. 14), NSE (Eq. 15) and RMSE (Eq. 16) are also applied so as to provide a better understanding of the performance of the models. In general, both hydrological models are able to satisfactorily capture the observed runoff for daily and monthly average runoff as shown in Table 5. During the calibration period (Table 5a), the table shows that the absolute difference of observed and simulated mean daily and monthly runoff values are smaller in the range between 0.001 and 0.215 m^3/s. This trend is similar with the SD and skewness. In terms of maximum runoff, both models give a large absolute difference in the maximum of observed and simulated runoff in the range of 0.248–39.275 m^3/s. Each model also offers a satisfactory performance of calibration result with the *R* and NSE coefficients ranging between 0.831–0.886 and 0.690–0.757, respectively. The performance is also supported with another performance index in which RMSE gives a smaller value with ranges between 4.975 and 7.478 m^3/s.

For validation periods (Table 5b), the table shows that the performances of the ANN and IHACRES models drop slightly compared to the performances of the models during the calibration period. It is seen that the absolute values of difference between the mean, SD and skewness are still smaller and accepted. In terms of performances indices, the models show satisfactory performance during the validation periods by the given *R* and NSE coefficients which range between 0.761–0.909 and 0.554–0.795, respectively. The RMSE is slightly larger compared to the RMSE during the calibration period with values ranging between 5.692 and 11.841 m^3/s.

To enhance the confidence of application of the models in this study, the performance during the testing period is proposed as shown in Table 5c. As demonstrated in the table, the performance during the testing period decreased compared to the performance of the models during the calibration and validation periods. It can be seen that the IHACRES model tends to replicate the observed daily and monthly average runoff in which the absolute differences are 1.334 and 1.609 m^3/s, respectively as compared to the ANN model. There are no differences in SD and skewness

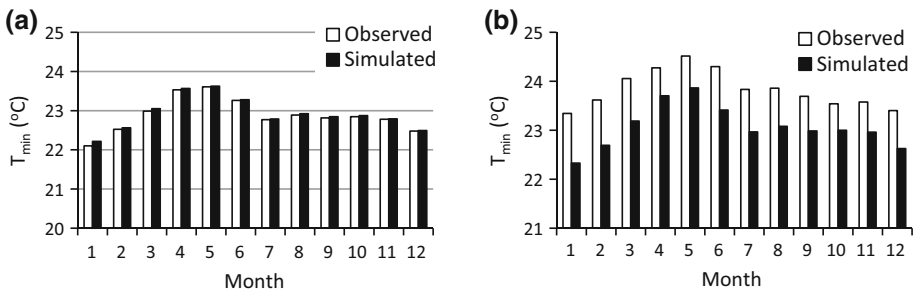

Fig. 5 Performance of the SDSM model on minimum daily temperature (T_{min}) during **a** calibration (1968–1989) and **b** validation (1989–2001) periods

Table 5 Comparative performance of the ANN and IHACRES models

	Daily			Monthly		
	Observed	ANN	IHACRES	Observed	ANN	IHACRES
(a) Calibration						
Mean (m^3/s)	16.702	16.678	16.907	16.651	16.652	16.866
SD (m^3/s)	13.428	11.353	10.861	10.102	7.257	7.959
Skewness	1.671	1.867	1.844	0.803	1.039	1.177
Maximum (m^3/s)	137.720	99.687	98.445	52.312	43.411	52.065
R		0.836	0.831		0.886	0.868
NSE		0.699	0.690		0.757	0.747
RMSE (m^3/s)		7.371	7.478		4.975	5.070
(b) Validation						
Mean (m^3/s)	20.198	17.466	21.390	20.104	17.422	21.327
SD (m^3/s)	17.736	12.989	14.253	12.631	7.311	9.596
Skewness	1.595	1.707	2.552	1.086	0.903	1.583
Maximum (m^3/s)	117.850	87.505	158.957	61.789	44.592	67.291
R		0.761	0.823		0.884	0.909
NSE		0.554	0.672		0.642	0.795
RMSE (m^3/s)		11.841	10.151		7.522	5.692
(c) Testing						
Mean (m^3/s)	19.615	17.926	21.049	19.345	17.790	20.954
SD (m^3/s)	21.017	12.980	12.557	12.068	7.581	8.782
Skewness	2.027	1.643	1.724	0.637	0.899	1.400
Maximum (m^3/s)	158.350	87.273	83.655	51.456	40.135	50.091
R		0.614	0.612		0.653	0.582
NSE		0.370	0.370		0.409	0.299
RMSE (m^3/s)		16.674	16.674		9.183	10.000

for each model with the absolute difference ranging between 3.286–8.460 and 0.263–0.763 m^3/s, respectively. This result is also clearly shown using the performance indices. The ANN and IHACRES models display moderate performance during the testing periods, in which the *R* and NSE are range from 0.582–0.653 to 0.299–0.409, respectively.

In terms of the model type, the ANN model seems to have a slightly higher performance compared to the IHACRES model based on the *R* and NSE coefficients as illustrated in Fig. 6. Although the ANN model gives the lowest value of *R* and NSE as compared to the IHACRES model during the validation period, the ANN model is able to provide the highest value during the testing period.

Generating synthetic daily rainfall and temperature corresponding to climate scenarios

Tables 6 and 7 illustrate the synthetic daily time series of rainfall and temperature produced for HadCM3 A2 and B2 scenarios using the SDSM model. The value of temperature was averaged from the T_{max} and T_{min} series. An assumption was made that the relationship between the predictor and predictand under the observed conditions remained valid under future climate conditions. Three periods of time, specifically, 2020s (2010–2039), 2050s (2040–2069) and 2080s (2070–2099) are defined. As illustrated in Table 6, the trend of change anomalies (differences) in mean daily rainfall against the current period (1981–1995) shows a similar trend, in which an increasing trend is shown in the daily rainfall particularly from January until February and April until November. In addition, those scenarios show a consistently decreasing trend in the daily rainfall during March and December. In particular, the daily rainfall fluctuated from period to period. The distinct changes were simulated to be matched during the period of the 2080s where May and November had a higher potential increase of daily rainfall, ranging from 12.18 to 16.31 mm from the current period. In the 2080s, the higher potential decrease of daily rainfall was shown to be in December with the value of 2.23 mm/day.

The change anomalies in the mean daily temperature corresponding to A2 and B2 scenarios are shown in Table 7. The daily mean temperature is an average of maximum and minimum daily temperature series. The B2 scenario projected an increase of +0.28 °C (November) in

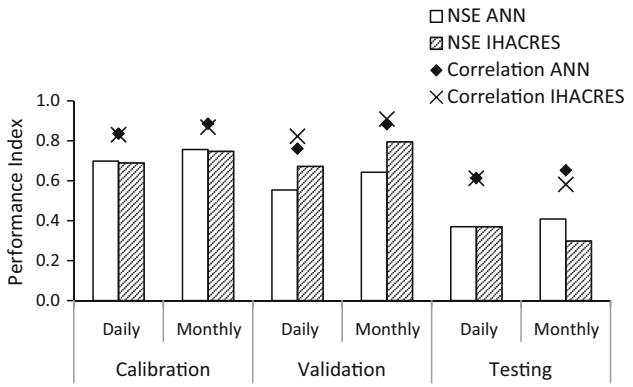

Fig. 6 Performance of ANN and IHACRES models based on correlation and NSE

Table 6 General trend of the change anomalies in mean daily rainfall corresponding to A2 and B2 scenarios

Months	A2			B2		
	2020s	2050s	2080s	2020s	2050s	2080s
1	0.50	1.14	2.16	0.83	0.89	1.00
2	1.09	2.27	6.04	1.41	1.92	3.74
3	−0.34	−1.23	−1.25	−0.23	−0.61	−0.83
4	2.53	2.71	3.58	2.54	3.01	3.36
5	1.55	5.78	12.19	0.94	4.31	8.73
6	0.48	0.47	0.18	0.29	0.37	0.39
7	3.25	3.87	5.09	2.88	3.58	4.44
8	1.70	2.23	2.85	1.67	2.29	2.53
9	1.56	5.01	10.00	1.81	4.04	7.09
10	2.29	4.06	6.28	2.01	2.91	4.55
11	4.25	8.91	16.31	3.86	7.01	12.72
12	−0.46	−1.68	−3.01	−0.11	−1.17	−2.23

the 2020s up to +1.25 °C (July) by the end of the century. The A2 scenario projected with higher change anomalies in the mean temperature than the B2 scenario, in which an increase was projected of +0.57 °C (July) in the 2020s and up to +2.02 °C in the 2080s.

Figures 7, 8 and Table 8a, b show the annual rainfall and temperature values corresponding to climate scenarios, respectively. The Kendall's Tau-b and Sen estimators were utilized (see "Evaluation and statistical analysis" section) to evaluate the rank correlation between each variable. As shown in Fig. 7 and Table 8a, increases in average and SD future rainfall (2011–2099) are recorded with the range of absolute differences between the observed and future rainfall for the A2 and B2 being 1,075.995 and 934.989 mm/years. The table shows that the future rainfall with A2 scenario projected with an increase of annual rainfall, with the rate (another analogy for Q_{mean}) of 18.478 mm/year with strong correlation ($\tau_b = 0.714$ and

Table 7 General trend of the change anomalies in mean daily temperature corresponding to A2 and B2 scenarios

Months	A2			B2		
	2020s	2050s	2080s	2020s	2050s	2080s
1	0.30	0.90	1.79	0.11	0.53	1.03
2	0.37	0.99	1.79	0.15	0.54	1.05
3	0.29	0.79	1.38	0.06	0.40	0.78
4	0.36	0.74	1.28	0.13	0.41	0.75
5	0.40	0.81	1.39	0.00	0.34	0.72
6	0.42	0.93	1.53	0.12	0.49	0.91
7	0.57	1.23	2.02	0.23	0.72	1.25
8	0.37	0.87	1.58	0.12	0.50	0.95
9	0.30	0.62	1.03	0.09	0.32	0.60
10	0.45	0.87	1.37	0.24	0.54	0.87
11	0.56	1.01	1.61	0.28	0.59	0.99
12	0.40	0.96	1.68	0.21	0.60	1.05

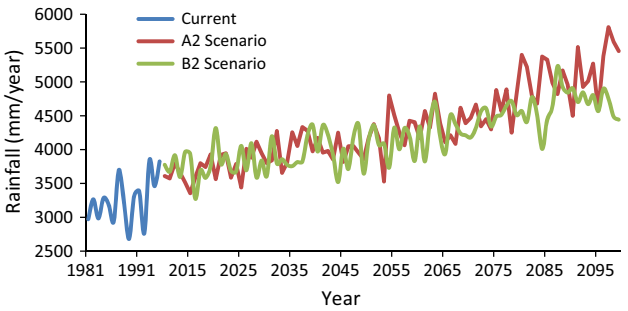

Fig. 7 General trend of the annual rainfall corresponding to A2 and B2 scenarios

p value = 0.000). The similar projected pattern of B2 scenario has been recorded, showing an increase of annual rainfall with the rate of 12.782 mm/year and statistically significant based on the Kendall's Tau-b ($\tau_b = 0.619$ and p value = 0.000).

In terms of annual temperature (Fig. 8; Table 8b), the SDSM model projected an increase of the average of annual temperature for the A2 and B2 scenarios with the absolute difference between the observed and projected values being 0.499 and 0.076 °C, respectively. The result also reveals that the A2 scenario gives a higher rate of annual temperature with the value of 0.019 °C at the end year of 2099, while the rate of B2 scenario is 0.013 °C. In addition, the Kendall Tau-b test indicates that these trends are statistically significant.

There are no true values alongside which to compare the projected values for future (Lee et al. 2010); hence, these results were compared with those from similar studies. The changes in mean rainfall and temperature were comparable to the results by MMD (2009) in the case of the A1B

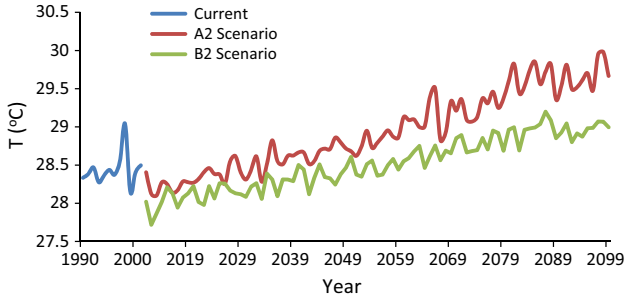

Fig. 8 General trend of the annual temperature (T) corresponding to A2 and B2 scenarios

scenario within the region of West-North Peninsular Malaysia. An increment of future annual rainfall and temperature was recorded by MMD (2009) and agreed with the studied result. This trend of increment was also consistent with results of Hassan et al. (2014a) and Kabiri et al. (2014) whose studies found an increment of rainfall and temperature being shown for the West-North area of Peninsular Malaysia.

Generating synthetic daily runoff corresponding to climate scenarios

The comparison of simulated change in the mean daily runoff values corresponding to downscaled data (rainfall and temperature) of the current (2006–2009) and future (2020s, 2050s and 2080s) climate is presented in Table 9. The results of possible future runoff generated from the two hydrological models by using the SDSM's results do not give identical results as shown in the table. The IHACRES model (Table 9a) seems to project a possible increase in the daily runoff in each period, whereas the ANN model (Table 9b) projected smaller changes in the daily runoff at the catchment's study area. In particular, the early months of the 2020s (January to September) show a higher increase of daily runoff projected by IHACRES and decrease of daily runoff at the end part of the 2020s for A2 and B2 scenarios. In the 2050s and 2080s, IHACRES projected an increase of daily runoff at each month, up to 52 (A2) and 36 m^3/s (B2). In contrast, the ANN model seems to project a small increase of daily runoff, but tends to give a large decrease of daily runoff especially at the end of these periods. The higher decrease of daily runoff projected by ANN is up to −15 (A2) and −14.8 m^3/s (B2), respectively. In terms of climate scenarios, the A2 scenario often shows a higher result for the fluctuation in runoff throughout the period, while the response of the B2 scenario to the runoff is likely to show an average result.

Figure 9 and Table 8c, d show the annual runoff corresponding to the A2 and B2 scenarios projected by the IHACRES and ANN models. The trends for the annual runoff were analysed using the Kendall's Tau-b and Sen estimators, similar to the trend analysis for annual rainfall and temperature. Based on the result (Fig. 9), the projected runoff of the IHACRES and ANN does not show an identical pattern for the annual trend. It can be seen that the IHACRES model produced a higher increase in annual runoff in each year, as compared to ANN. These trends are detailed in Table 8c, d with the rate of annual runoff produced by IHACRES shown as being significantly higher with rates being 0.247 and 0.187 m^3/s for the A2 and B2 scenarios, respectively. As compared to the rate of the annual runoff at the end of 2099 produced by ANN, the rates are 0.037 and 0.033 m^3/s for the A2 and B2 scenarios,

Table 8 Trend analysis using the Kendall's Tau-b and Sen estimator methods with $\alpha = 0.05$ for annual time series

	Average	n	τ_b	p value	Q_{mean}
(a) Rainfall (mm/annual)					
Current	3,255.192	15	0.352	0.075	37.592
2011–2099 (A2 Scenario)	4,331.187	90	0.714	0.000	18.478
2011–2099 (B2 Scenario)	4,190.181	90	0.619	0.000	12.782
(b) Temperature (°C)					
Current	28.439	12	0.273	0.244	0.011
2011–2099 (A2 Scenario)	28.938	89	0.832	0.000	0.019
2011–2099 (B2 Scenario)	28.515	89	0.807	0.000	0.013
(c) Runoff (IHACRES) (m^3/s)					
Current	20.173	10	0.156	0.592	0.197
2011–2099 (A2 Scenario)	31.027	89	0.770	0.000	0.247
2011–2099 (B2 Scenario)	28.686	89	0.725	0.000	0.187
(d) Runoff (ANN) (m^3/s)					
Current	20.173	10	0.156	0.592	0.197
2011–2099 (A2 Scenario)	19.776	89	0.417	0.000	0.037
2011–2099 (B2 Scenario)	19.634	89	0.434	0.000	0.033

Table 9 Simulated change anomalies in mean daily runoff of the ANN and IHACRES models driven by the A2 and B2 scenarios

Months	(a) IHACRES						(b) ANN					
	A2			B2			A2			B2		
	2020s	2050s	2080s	2020s	2050s	2080s	2020s	2050s	2080s	2020s	2050s	2080s
1	3.84	4.61	6.11	5.38	10.71	8.78	0.97	−0.05	−1.71	1.96	0.87	−0.62
2	6.22	6.50	9.07	8.90	16.89	13.40	4.72	2.42	4.13	4.71	3.91	4.28
3	8.39	7.94	8.01	8.98	14.27	12.71	4.72	1.16	−1.10	4.03	3.66	1.21
4	7.90	7.43	7.20	9.40	12.57	11.15	2.70	3.09	3.23	2.14	3.80	4.27
5	8.31	7.12	20.83	16.71	41.79	31.15	−2.47	3.82	12.31	−2.86	2.27	7.68
6	1.56	1.14	5.64	4.60	12.16	9.52	−2.79	−5.51	−7.83	−3.47	−4.37	−6.00
7	7.99	7.00	11.08	10.17	17.63	14.99	5.38	4.74	4.71	4.61	4.74	4.99
8	2.81	2.36	6.82	6.22	12.74	10.04	−1.16	−1.00	−2.04	−0.97	−0.99	−1.22
9	0.08	0.27	7.10	5.21	18.84	12.68	−0.25	3.62	7.76	−0.34	2.66	5.88
10	−3.01	−3.33	6.23	1.56	19.94	10.70	−4.93	−1.69	2.03	−5.70	−4.22	0.38
11	5.09	2.66	21.38	14.49	52.26	36.73	−9.60	−5.18	0.31	−9.89	−6.78	1.22
12	−2.87	−2.20	1.58	−0.73	9.37	6.98	−11.18	−14.17	−15.84	−10.70	−13.14	−14.78

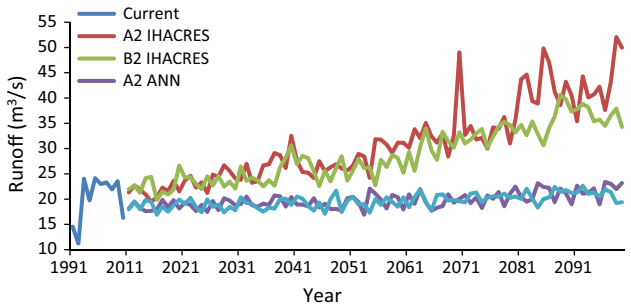

Fig. 9 General trend of the annual runoff corresponding to A2 and B2 scenarios

respectively. The trends produced by both models showed a strong correlation evaluated by the Kendall Tau-b method ($\tau_b > 0.400$ and p value $= 0.000$).

Discussion

Changes in climate will have significant impacts on water resources and hydrological regimes. This study focused on the small sub-catchment area known as the Kurau River which is located in the northern area of Peninsular Malaysia. Daily rainfall and temperature are climate variables that have been chosen as the focus of the study. Observed data of 30–35 years were applied in order to generate future rainfall and temperature data by using the selected predictors (GCMs variables) for the hydrological models. The SDSM, which utilized the statistical downscaling approaches, was applied for this purpose. Those simulated climate variations which corresponded to the climate scenarios became the inputs for the hydrological models by which to assess potential impacts of climate change on river runoff. Two climate scenarios (A2 and B2) were considered to take into account the prediction uncertainty due to the used emission scenario.

The SDSM concept is the recognition of the empirical relationship between the gridded predictors and single-site predictand factors (temperature and rainfall). It is the most difficult and challenging part of downscaling due to the temporal and spatial variation of the explanatory power of each predictor (Wilby et al. 2002). NCEP data were re-gridded and normalized towards the grid-system HadCM3 for the purposes of calibration. The selection of the NCEP variables for calibration depends on the correlation and inter-relationship between the predictand and predictor pairs. The correlation and partial correlation values (Table 2) are used to study the relationship between the NCEP variables to the predictands. As shown in the result, the selection of the NCEP variables is difficult to finalize due to lower correlation and insignificance existing between the pairs. This can be attributed to the conditional process (wet and dry days) inside the rainfall and is affected by different variables (Kabiri et al. 2014; Hassan et al. 2014a; Dibike and Coulibaly 2005). Although the choice of predictors for rainfall does not offer a significant statistical comparison between the downscaled and observed rainfall during the calibration and validation periods, nevertheless a good result was given (as shown in Fig. 3). In terms of the downscaling of T_{max} and T_{min} (Fig. 4 and 5), the performance is slightly better than the performance of downscaled daily rainfall using the list of predictors in Table 2. Similar studies such as Fealy and Sweeney (2007),), Khan et al. (2006), Dibike and Coulibaly (2005) and Wilby et al. (2002) found that the daily

temperature is easy to downscale as compared to daily rainfall due to the existence of continuous variables. In addition, it is less affected by time irregularities (as studied in detail by Hassan et al. 2014a).

With respect to future trends, the SDSM simulated an increase in daily rainfall (Table 6) of the Kurau sub-catchment by the 2080s with the highest values being in May and November (up to +16.31 mm), and the lowest decrease in December (up to −2.23 mm). At the same time, IHACRES (Table 9a), which utilized a hybrid metric-conceptual-based model based on downscaled rainfall and temperature, showed an increasing value of daily river runoff in May and November within the range of 42–31 and 52–37 m^3/s, respectively.

Since there is no correct way to validate future performance on river runoff, this subsequently becomes a major uncertainty in this study. The results of IHACRES were compared with the metric-based model, namely ANN, in an attempt to overcome this uncertainty. Calibration and evaluation (validation and testing) were performed using the observed data with the similar data periods of IHACRES. With sufficient data sets (Eq. 13), the ANN model can be trained (calibrated) and managed so as to give a better performance than that of IHACRES in the evaluation period. From the early investigation by (Hassan et al. 2014b), it can be seen that the increase of data sets (such as those in a number of antecedent rainfall and/or antecedent temperature data) is not an assurance of ANN's better performance. Since the ANN model is a data-driven technique, the response between input and output of ANN is simple to understand, as compared to the physical and/or conceptual models. A total of 20 daily time series were used in order to train the ANN model to be able to replicate present and future conditions. In terms of future trends in daily series, the river runoff simulated by ANN (Table 9b) provides smaller changes in river flow, in the range of −16 to 12 m^3/s. During May–June and October–December, the decrease of river runoff simulated by the ANN model is recorded. This situation reflects the decreasing pattern of rainfall and temperature.

The comparisons of the trend of annual runoff simulated by the IHACRES and ANN models are clearly seen in the visual comparison in Fig. 9 and Table 8c, d. The comparisons clearly show the projection of future annual runoff between both models not showing any identical result. The study found IHACRES produced a significant higher rate of future annual runoff as compared to the ANN model. This circumstance occurs due to the differing methods used by each model in handling input of the models. In theory, an increase of rainfall intensity will subsequently escalate the rate of runoff, and vice versa. This situation is clearly shown in the generation of runoff simulated by the IHACRES model in which the annual rate of runoff for 2011–2099 in the range between 0.187 and 0.247 m^3/s is influenced by the increment of rainfall intensity in the range 12.782–18.478 mm/years. Although there is a slight increase in the rate of annual temperature in the range between 0.013 and 0.019 °C, the modules in the IHACRES model which transform the temperature to evaporation offer less significance towards the change in the rate of annual runoff.

This trend pattern is not followed by the ANN model, which shows a slight increase in the rate of annual runoff with the value of 0.033–0.037 m^3/s (Table 8d). Since the calibration of the ANN model does not consider the hydrological process as compared to the IHACRES model, the output of ANN can be relative based on input–output patterns recognized through learning (calibration) (Gupta and Singh, 2011). In this study, the temperature series (including the antecedent temperature) became a dominant input in this model. This was detailedly shown in Eq. 13, similar to the rainfall series. This situation leads to smaller increases in the rate of future annual runoff, as well as daily runoff series due to the influence of higher increases in future temperature series. The ANN model was able to well reproduce the observed runoff during the validation and testing periods (Table 5b, c). However, the simulation of runoff for the future (corresponding to the climate scenarios) can be questionable when not shown identical patterns of anomalies in mean daily rainfall and annual trends (based on the Kendall's Tau-b and Sen estimator).

Conclusion

This study compared the relative ability of the IHACRES and ANN models to reproduce levels of present and future runoff using the input from the downscaled rainfall and temperature values from the SDSM. In general, the wet and warm climates would result in significant changes in the increase of daily river runoff in the sub-catchment of the Kurau River, Malaysia. Increments in the annual rainfall rate in the range of 12.782–18.478 mm/year for most daily runoff of projected data by hydrological models in each month are shown in this study. Although the increment of annual temperature rate in the range of 0.011–0.019 °C/year is recorded for a future scenario, this does not lead to a decrease in future river runoff. The higher depth of future rainfall and insignificance of temperature effect projected a higher peak runoff, and those events can contribute to future flood events in the downstream of the sub-catchment. Therefore, water and flood management planning is key challenges faced by the local authorities.

In terms of the application of the ANN model, results reveal that the model does not provide an identical trend of analysis as compared to the IHACRES model. Although

the ANN model is able to reproduce the current observed similarly to the IHACRES model, it is not able to produce a similar trend of runoff series such as the runoff projected by the IHACRES model. It is not recommended to use this model solely as an application for a hydrological model, nor is it recommended to project runoff or discharge in the climate change assessment. A combination of careful attention and calibration processes is needed for that purpose.

The physiographic characteristic of the case study contributed to the limitations of the study since the physical properties (e.g. topography and soil permeability) of the river catchment were not considered. Hence, the study recommends that future researchers apply the physical hydrological models for river runoff estimation. It is anticipated that this would allow an assessment based on the result from different types of hydrological models. An adjustment to the current ANN model, which includes the physical properties, should be considered to enhance the quality of river runoff. Since this study used the data from one catchment, it is considered, therefore, that further studies should be performed for generalization of results.

In addition, it is expected that future studies can be performed concerning the exploration of the impact of climate change on various sectors including crop production and reservoir assessment. Hence, a list of adaptation factors for climate change can be proposed.

Acknowledgments The first author is grateful to Universiti Malaysia Perlis and the Ministry of Education Malaysia for the opportunity of study leave at Universiti Teknologi Malaysia. Thanks are also extended to the Department of Irrigation and Drainage Malaysia for providing the data and technical support.

References

Nakićenović N et al (2000) Emissions scenarios. A special report of working group III of the intergovernmental panel on climate change. Cambridge University Press, Cambridge

Bernard B, Vincent K, Frank M, Anthony E (2013) Comparison of extreme weather events and streamflow from drought indices and a hydrological model in River Malaba, Eastern Uganda. Int J Environ Stud 70(6):940–951

Chu JT, Xia J, Xu CY, Singh VP (2010) Statistical downscaling of daily mean temperature, pan evaporation and precipitation for climate change scenarios in Haihe River, China. Theoret Appl Climatol 99(1–2):149–161

Combalicer E, Cruz R, Lee S (2010) Assessing climate change impacts on water balance in the Mount Makiling forest, Philippines. J Earth Syst 3:265–283

Coulibaly P, Dibike YB (2005) Downscaling precipitation and temperature with temporal neural networks. J Hydrometeorol 6:483–496

Croke BFW, Jakeman AJ (2004) A catchment moisture deficit module for the IHACRES rainfall-runoff model. Environ Model Softw 19:1–5

Croke BFW, Andrews F, Jakeman AJ, Cuddy SM, Luddy A (2006) IHACRES classic plus: a redesign of the IHACRES rainfall-runoff model. Environ Model Softw 21:426–427

Dawson CW, Wilby RL (2001) Hydrological modelling using artificial neural networks. Prog Phys Geogr 25(1):80–108

Dibike YB, Coulibaly P (2005) Hydrologic impact of climate change in the Saguenay watershed: comparison of downscaling methods and hydrologic models. J Hydrol 307(1–4):145–163

Dibike YB, Solomatine DP (2001) River flow forecasting using artificial neural networks. Phys Chem Earth B Hydrol Oceans Atmos 26(1):1–7

Fealy R, Sweeney J (2007) Statistical downscaling of precipitation for a selection of sites in Ireland employing a generalised linear modelling approach. Int J Climatol 27(15):2083–2094

Gibson JK, Kallberg P, Uppala S, Hernandez A, Nomura A, Serrano E (1999) ECMWF re-analysis project report series. European Centre for Medium-Range Weather Forecasts

Gordon C, Cooper C et al (2000) The simulation of SST, sea ice extents and ocean heat transports in a version of the Hadley Centre Coupled Model without flux adjustments. Clim Dyn 16(2):147–168

Gupta A, Singh Y (2011) Analysis of feature recognition of neural network method in the string recognition. In: Nagamalai D, Renault E, Dhanuskodi M (eds) Advances in parallel distributed computing SE-62. Communications in computer and information science. Springer, Berlin, pp 638–647. doi:10.1007/978-3-642-24037-9_62

Hassaballa AA, Matori AB (2011) The estimation of air temperature from NOAA/AVHRR images and the study of NDVI-Ts impact. Case study: the application of split-window algorithms over (Perak Tengah and Manjong) area, Malaysia. In: Proceeding of the 2011 IEEE international conference on space science and communication (IconSpace) 12–13 July 2011, Penang, Malaysia, pp 20–24

Hassan Z, Harun S (2012) Application of statistical downscaling model for long lead rainfall prediction in Kurau River catchment of Malaysia. Malays J Civil Eng 24(1):1–12

Hassan Z, Shamsudin S, Harun S (2014a) Application of SDSM and LARS-WG for simulating and downscaling of rainfall and temperature. Theoret Appl Climatol 116(1–2):243–257. doi:10.1007/s00704-013-0951-8

Hassan Z, Shamsudin S, Harun S (2014b) Minimum input variances for modelling rainfall-runoff using ANN. Jurnal Teknologi (Sci Eng) 69(3):113–118

Hsu KL, Gupta HV, Sorooshian S (1995) Artificial neural network modelling of the rainfall-runoff process. Water Resour Res 31(10):2517–2530

Jiang T, Chen YD, Xu C, Chen X, Singh VP (2007) Comparison of hydrological impacts of climate change simulated by six hydrological models in the Dongjiang Basin, South China. J Hydrol 336:316–333

Kaas E, Frich P (1995) Diurnal temperature range and cloud cover in the Nordic countries: observed trends and estimates for the future. Atmos Res 37:211–228

Kabiri R, Bai VR, Chan A (2014) Assessment of hydrologic impacts of climate change on the runoff trend in Klang Watershed. Environ Earth Sci, Malaysia. doi:10.1007/s12665-014-3392-5

Kalnay E et al (1996) The NCEP/NCAR 40-year reanalysis project. Bull Am Meteorol Soc 77:437–471

Karamouz M, Fallahi M, Nazif S, Rahimi Farahani M (2012) Long lead runoff simulation using data-driven models. Int J Civil Eng 10(4):328–336

Kendall M (1938) A new measure of rank correlation. Biometrika 30:81–89

Khan MS, Coulibaly P, Dibike Y (2006) Uncertainty analysis of statistical downscaling methods. J Hydrol 319(1–4):357–382. doi:10.1016/j.jhydrol.2005.06.035

Kokkonen T, Jakeman AJ, Young PC, Koivusalo HJ (2003) Predicting daily flows in ungauged catchments: model regionalization from catchment descriptors at the Coweeta Hydrologic Laboratory, North Carolina. Hydrol Process 11:2219–2238

Lee E, Seong C, Kim H, Park S, Kang M (2010) Predicting the impacts of climate change on nonpoint source pollutant loads from agricultural small watershed using artificial neural network. J Environ Sci 22(6):840–845

Littlewood IG, Down K, Parker JR, Post DA (1997) IHACRES—catchment-scale rainfall-streamflow modelling (PC version) Version 1.0: April 1997. The Australian National University, Institute of Hydrology and Centre for Ecology and Hydrology

Minns AW, Hall MJ (1996) Artificial neural networks as rainfall-runoff models. Hydrol Sci J 41(3):399–416

MMD (2009) Scientific report: climate change scenarios for Malaysia. Jalan Sultan, Petaling Jaya. http://www.met.gov.my/images/pdf/nwp/climate-scenarios.pdf. Accessed 24 July 2012

Mollema P, Antonellini M (2012) Climate and water budget change of a Mediterranean coastal watershed, Ravenna, Italy. Environ Earth Sci 65:257–276. doi:10.1007/s12665-011-1088-7

Nor N, Harun S, Kassim A (2007) Radial basis function modelling of hourly streamflow hydrograph. J Hydrol Eng 12(1):113–123

Poccard I, Janicot S, Camberlin P (2000) Comparison of rainfall structures between NCEP/NCAR reanalyses and observed data over tropical Africa. Clim Dyn 16(12):897–915

Puka L (2011) Kendall's tau. In: Lovric M (ed) International encyclopedia of statistical science SE-324. Springer, Berlin, pp 713–715

Samadi S, Carbone GJ, Mahdavi M, Sharifi F, Bihamta MR (2012) Statistical downscaling of climate data to estimate streamflow in a semi-arid catchment. Hydrol Earth Syst Sci Discuss 9(4):4869–4918

Samadi S, Carbone GJ, Mahdavi M, Sharifi F, Bihamta MR (2013) Statistical downscaling of river runoff in a semi-arid catchment. Water Resour Manage 27:117–136

Sen PK (1968) Estimates of the regression coefficient based on Kendall's tau. J Am Stat Assoc 63:1379–1389

Tokar AS, Johnson PA (1999) Rainfall runoff modelling using artificial neural networks. J Hydrol Eng 4(3):232–239

Tukimat NNA, Harun S, Shahid S (2012) Comparison of different methods in estimating potential evapotranspiration at Muda Irrigation Scheme of Malaysia. J Agric Rural Dev Trop Subtrop 113(1):77–85

Wilby RL (2005) Uncertainty in water resource model parameters used for climate change impact assessment. Hydrol Process 19(16):3201–3219

Wilby RL, Dawson CW (2013) The statistical downscaling model: insights from one decade of application. Int J Climatol 33(7):1707–1719

Wilby RL, Harris I (2006) A framework for assessing uncertainties in climate change impacts: low-flow scenarios for the River Thames, UK. Water Resour Res 42(2):W02419. doi:10.1029/2005WR004065

Wilby RL, Wigley TML (1997) Downscaling general circulation model output: a review of methods and limitations. Prog Phys Geogr 21:530–548

Wilby RL, Dawson CW, Barrow EM (2002) SDSM—a decision support tool for the assessment of regional climate change impacts. Environ Model Softw 17:147–159

Xu CY (1999) From GCMs to river flow: a review of downscaling methods and hydrologic modelling approaches. Prog Phys Geogr 23(2):229–249

Ye W, Bates BC, Viney NR, Sivapalan M, Jakeman AJ (1997) Performance of conceptual rainfall-runoff models in low-yielding ephemeral catchment. Water Resour Res 33:153–166

Zadeh MR, Amin S, Khalili D, Singh VP (2010) Daily outflow prediction by multi-layer perceptron with logistic sigmoid and tangent sigmoid activation. Water Resour Manage 24(11):2673–2688

Zareian MJ, Eslamian S, Hosseinipour EZ (2014) Climate change impacts on reservoir inflow using various weighting approaches. World Environ Water Resour Congr 2014:2136–2145. doi:10.1061/9780784413548.213

Zarghami M, Abdi A, Babaeian I (2011) Impacts of climate change on runoffs in East Azerbaijan, Iran. Global Planet Change 78(3–4):137–146

Zhang GP, Savenije HHG (2005) Rainfall-runoff modelling in a catchment with a complex groundwater flow system: application of the Representative Elementary Watershed (REW) approach. Hydrol Earth Syst Sci 9:243–261